Journal of Electroceramics 4:S1, 113–120, 1999

Effect of Silica Doping on the Electrical Conductivity of 3 mol % Yttria-Stabilized Tetragonal Zirconia Prepared by Colloidal Processing

T. UCHIKOSHI, Y. SAKKA & K. HIRAGA

National Research Institute for Metals, 1-2-1 Sengen, Tsukuba, Ibaraki 305-0047, Japan

Submitted November 14, 1997; Revised January 21, 1999; Accepted March 30, 1999

Abstract. Silica-doped ($SiO_2 = 0 - 1.0$ wt %) 3Y-TZP (3 mol % yttria-doped tetragonal zirconia polycrystal) ceramics are prepared from hetero-coagulated aqueous suspension by colloidal processing. Consolidation of the suspension was carried out by pressure filtration at 10 MPa followed by cold isostatic pressing (CIP) at 400 MPa. Consolidated compacts are densified to a relative density over 99% by sintering at 1573 K for 2 h. The formation of glass pockets at grain boundary multiple junctions was observed by SEM for ≥ 0.5 wt % silica-doped samples. Electrical conductivity measurements were performed to evaluate the modification of grain-boundaries by silica. The apparent grain boundary conductivity decreased with an increase in silica content and became nearly constant above 0.3 wt % of silica, while the bulk conductivity was constant with silica content.

Keywords: tetragonal zirconia, yttria, silica, electrical conductivity

1. Introduction

Yttria-doped tetragonal zirconia polycrystal (Y-TZP) is known as a material that demonstrates superplasticity [1–3]. This property is greatly affected by the microstructure of the sintered body, and becomes evident at small grain sizes of less than 1 μm. The extensive tensile elongation up to 800% has been reported for 3Y(3 mol % Y_2O_3)-TZP, with an initial grain size of about 0.3 μm [4]. The intergranular phase at grain boundaries promotes the decrease in flow stress and the enhancement of tensile ductility for TZP [5,6]. Silica-doping is very effective in improving the superplasticity of TZP. Kajihara et al. [7] have reported a maximum elongation of over 1000% at 1673 K for 5 wt % SiO_2-doped 2.5 Y-TZP. Hiraga et al.[8] have investigated the tensile creep behavior of SiO_2-doped 3Y-TZP and reported that an increase in fracture strain is observed for samples with >1 wt % of SiO_2, but a reduction in flow stress is observed for ≤ 0.3 wt % of SiO_2. Their result shows that the addition of small amounts (up to 0.3 wt %) of silica determines the initial stage of superplasticity of TZP.

Pore sizes and their distribution are very important factors that determine the mechanical properties of sintered ceramics. Large pores are often the starting points for fracture. Therefore, a uniform particle packing of green compacts is required. Colloidal processing is a powerful method for controlling the density and microstructure of a consolidated compact [9–11]. Particle packing is influenced by interparticle forces. These forces can be changed from attractive to repulsive by adjusting the pH of the aqueous suspension. Attractive potentials among particles help to prevent segregation. On the other hand, repulsive potentials contribute to a dense packing of particles. Moreover, if the grain boundaries of TZP are modified with silica uniformly and the defects in the sintered body are minimized, then excellent superplasticity of TZP can be expected, even if the amount of silica is less than 1 wt %.

Yttria-doped zirconia is an excellent solid electrolyte material and many studies have been reported on the conductivity properties [6,12–21]. In typical

polycrystalline stabilized zirconia, both the intragrain and the grain boundaries contribute to the total resistance. Impedance spectroscopy has been widely used to separate the intragrain and grain boundary contributions. It has been reported that silica decreases the grain boundary conductivity of zirconia [17]. Therefore, the measurement of the grain boundary conductivity of 3Y-TZP is useful to characterize the segregation of silica at grain boundaries.

In the present work, silica-doped 3Y-TZP ceramic with (1) uniform modification of zirconia with silica and (2) homogeneous microstructure from nano-sized powder was prepared by colloidal processing. The electrical conductivity was measured for 3Y-TZP with different silica contents by the complex impedance method.

2. Experimental

The experimental work was performed using 3 mol% yttria-doped tetragonal zirconia (3Y-TZ) powder (Tosoh. Corp., TZ3Y; average particle size is 60 nm) and colloidal silica (Nissan Chem. Ind., Ltd., Snowtex O; particle size of 10–20 nm). The impurities of the 3Y-TZ are 0.005 wt % Al_2O_3, 0.004 wt % SiO_2, 0.002 wt % Fe_2O_3 and 0.013 wt % Na_2O. The main impurity of the colloidal silica is 0.032 wt % Na_2O. The aqueous suspension of the zirconia-silica system was prepared at pH = 5.3. The solid content of the suspension was fixed at 7 vol %. For pH adjustment, 1N HNO_3 and 1N NH_4OH solutions were used. Figure 1 shows the ζ-potential versus pH of 3Y-TZ and silica powders measured by a laser electrophoresis ζ-potential analyzer (Otsuka Electronics Co., LEZA-600) [22]. The isoelectric points of the zirconia and silica are at pH = 7.2 and 2.6, respectively. The ζ-potential represents the interparticle potential in a suspension. At pH = 5.3, the interparticle forces between ZrO_2-ZrO_2 and SiO_2-SiO_2 are repulsive, but those for ZrO_2-SiO_2 are attractive. Therefore a heterocoagulated condition, i.e., uniform modification of zirconia particles by silica particles, is expected. The suspensions were ultrasonicated for 10 min and stirred by a magnetic stirrer for 12 h at room temperature. The silica content was varied between 0-1.0 wt % against zirconia.

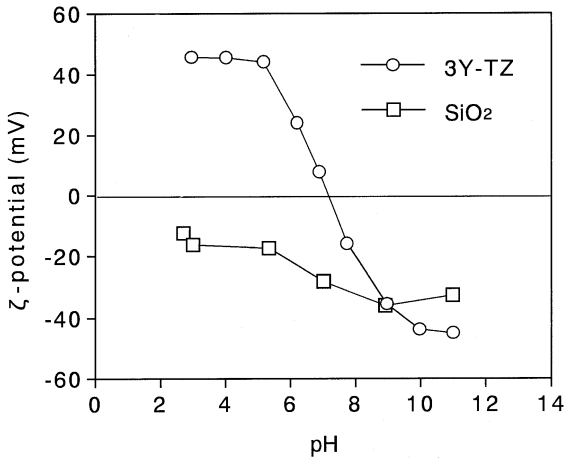

Fig. 1. Effect of pH on the ζ-potential of 3Y-tetragonal zirconia and colloidal silica in aqueous suspensions.

The consolidation of the suspension was performed by pressure filtration (PF) [10,11,23,24] at 10 MPa. Before the consolidation, the suspension was evacuated in a vacuum desiccator to eliminate air bubbles. The details of the pressure filtration process have been reported elsewhere [23]. A Teflon membrane with pores of 0.1 μm was used as a filter. CIP treatment at 400 MPa was carried out to improve the packing density of the green compacts after the consolidation by pressure filtration. The green compacts were disc shaped and the diameter and thickness were 50 mmϕ and 3–4 mm, respectively. The compacts were dried overnight at 393 K, and sintered in air at 1573 K for 2 h. The relative green density of the sintered bodies was measured by the Archimedes' method to be above 99% for all the samples.

The microstructure of the sintered bodies was observed by SEM (JEOL JSM-840F) for polished and chemically and thermally-etched surfaces. Chemical etching was performed by soaking the polished surface in a mixture of $HF : H_2SO_4 : H_2O = 1 : 4 : 20$ for 2 min. Thermal etching was performed in air at 1523 K for 20 min after the chemical etching.

Conductivity measurements were carried out using an impedance analyzer (Hewlett Packard HP 4194A) in air over the frequency range of 100 Hz to 15 MHz. Rectangular parallelepiped samples, 4–5 mm long, 4–5 mm wide and 1–2 mm thick, were cut out from the sintered bodies. Platinum electrodes were applied to the samples using a conductive platinum paste and were sintered onto the surface at 1273 K for 1 h.

3. Results and Discussion

3.1. Microstructure

Figure 2 shows the microstructure of the compacts sintered at 1573 K for 2 h. The average grain size, determined by the linear intercept method [25], is shown in Table 1. The grain sizes of the sintered compacts are almost the same regardless of the amount of silica. The intergranular phase promotes the sintering of TZP ceramics at high temperatures because of the formation of a liquid phase [26]. On the contrary, solid phase sintering of TZP at 1473 K is suppressed by silica-doping [22]. Though the sintering temperature of 1573 K must be lower than the temperature of liquid phase formation, no obvious data were obtained for the suppression of TZP sintering. For those compacts with silica content ≥ 0.5 wt %, some pores were observed at grain multiple junctions. Those pores were observed only for surfaces chemically etched by hydrofluoric acid. Therefore, the pores are traces of the excess amount of silica segregated at grain boundary multiple junctions.

To clarify the mechanism of superplasticity of silica-doped TZP, the characterization of the grain boundaries is very important. The presence or absence of continuous amorphous layers at grain boundaries has been one of issue that must be settled. Earlier studies supported the presence of the intergranular glassy phase [18,28], whereas some recent studies by

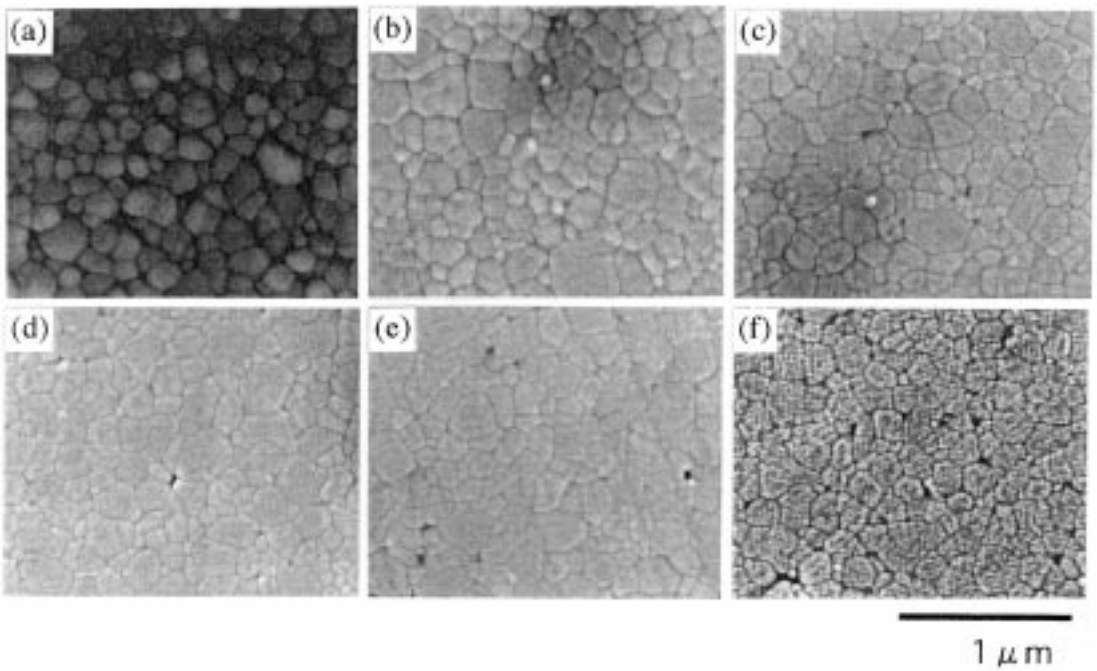

Fig. 2. Microstructure of silica-doped 3Y-TZP sintered at 1573 K for 2 h: (a) undoped, (b) 0.1 wt % SiO_2, (c) 0.3 wt % SiO_2, (d) 0.5 wt % SiO_2, (e) 0.7 wt % SiO_2 and (f) 1.0 wt % SiO_2.

Table 1. Density, average grain size, activation energies of the total bulk and the total grain boundary conductivities

Sample	Density (g/cm^3)	Grain size (μm)	E_b (eV)	E_{gb} (eV)
Undoped 3Y-TZP	6.03	0.23	0.91	1.02
3Y-TZP-0.1% SiO_2	6.04	0.23	0.93	1.10
3Y-TZP-0.3% SiO_2	6.03	0.24	0.90	1.07
3Y-TZP-0.5% SiO_2	6.01	0.23	—	—
3Y-TZP-0.7% SiO_2	6.00	0.24	—	—
3Y-TZP-1.0% SiO_2	5.95	0.23	0.92	1.06

HREM observation support the absence of the glassy phase [20,27]. Ikuhara et al. [27] have reported that no continuous amorphous phase is observed at the grain boundaries even in 5 wt % pure silica-doped 3Y-TZP. They have also reported that silicon and yttrium segregate across the grain boundaries over a width of several nm. Hiraga et al. [8] observed the grain boundaries of silica-doped 3Y-TZP by TEM and reported the existence of paired Fresnel fringes at most of the two grain junctions by over- or under-focused imaging operation. They did not find the paired Fresnel fringes in the undoped 3Y-TZP. Therefore, assuming that the paired fringe appeared at the places where the inner potential is lower than that of matrix grains, they have estimated the thickness of the intergranular phase to be 0.8 nm by Clarke's method [29]. Considering those studies, it is probable that the solute-segregated phase is formed at grain boundaries.

Solute coverage is calculated in terms of equivalent monolayers [20,30]. For tetrakaidechahedral (14-sided polyhedral) grains of longnormal grain-size distribution, the total grain boundary area per unit volume of sample (S_v) is given by

$$S_v = 3.11/d_g \quad (\mathrm{cm}^2) \tag{1}$$

where d_g is the average grain size (cm). The total number of silicon atoms in a unit volume of SiO_2-doped 3Y-TZP is given by

$$\begin{aligned} N_{si} &= N_A \times (\rho[\mathrm{SiO_2}]/60.08) \\ &= 1.00 \times 10^{22} \rho[\mathrm{SiO_2}] \quad (\text{atoms}) \end{aligned} \tag{2}$$

where ρ is the density $(\mathrm{g/cm}^3)$, $[SiO_2]$ the overall concentration of silica in weight fraction. If it is assumed that there is no bulk solubility of silica and the coverage of silica at a grain boundary is uniform, the silicon coverage at a grain boundary is obtained as

$$\Gamma_{Si} = 3.22 \times 10^{21} \rho[\mathrm{SiO_2}] d_g \quad (\mathrm{atoms/cm}^2) \tag{3}$$

Figure 3 shows the silicon coverage versus the amount of doped silica. A silica content of 0.004 wt % is used for the undoped 3Y-TZP.

One monolayer of cation segregation at grain boundaries, assuming each cation site to be available for substitution by the solute, is calculated as $N_v^{2/3}$, where N_v is the lattice cation site density [20,30]. N_v for 3 mol % Y_2O_3-stabilized ZrO_2 is calculated as $1.48 \times 10^{22} (\mathrm{atoms/cm}^3)$ using $a_0 = 0.5102$ nm and $c_0 = 0.5175$ nm for the lattice constants of 3Y-TZP [31]. Therefore one monolayer of cation site is estimated as $6.04 \times 10^{14} (\mathrm{atoms/cm}^2)$. The monolayer level of silicon is also indicated in Fig. 3. If it is assumed that the width of the grain boundary layer is 0.8 nm [8] and all the sub-grain boundary cation sites are occupied with silicon atoms, the equivalent silicon-segregated layer is roughly estimated as $0.8/(c_0/2) = 2.8$ monolayers and the equivalent SiO_2 content is estimated to be 0.37 wt % from Fig. 3.

3.2. Conductivity Measurement

Figure 4 shows the complex impedance spectra at 670 K for the samples with different silica contents. Two clear semicircles are obtained for all the samples. The equivalent circuit is also shown in this figure. Generally, the impedance $Z(= Z' - jZ'')$ of polycrystalline ceramics is given as the sum of the impedances of domains i, bulk (and surface) and grain boundary.

$$Z = \sum Z_i = \sum (R - jX)_i \tag{4}$$

where, R, X and j are resistance, reactance and imaginary number unit, respectively. The first semicircle at higher frequency and the second semicircle at lower frequency are attributed to the bulk and the grain boundary contributions, respectively. Therefore, the intersections of the extrapolated lines of the semicircles with the Z' axis in Fig. 4 give the resistivities originating from the bulk grains and

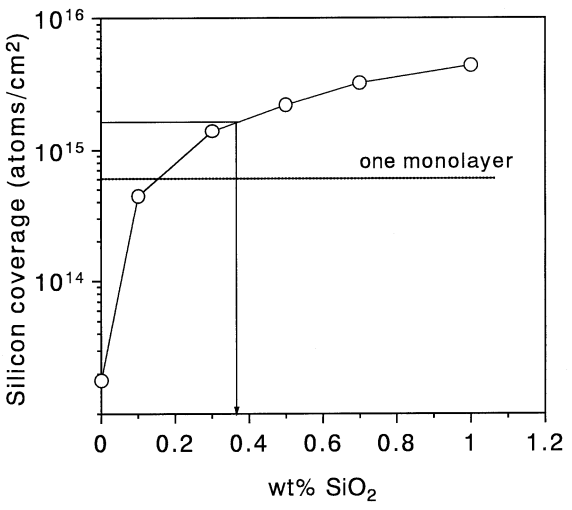

Fig. 3. Average silicon coverage at grain boundaries versus silica content.

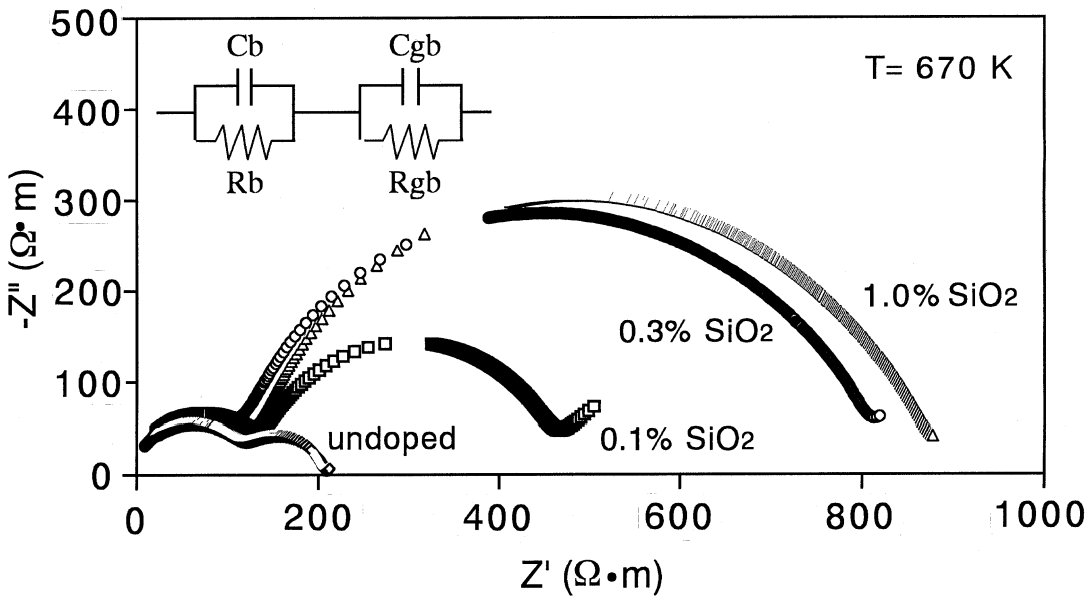

Fig. 4. Complex impedance spectra of the samples with various silica contents. The equivalent circuit of the spectra is shown as inset.

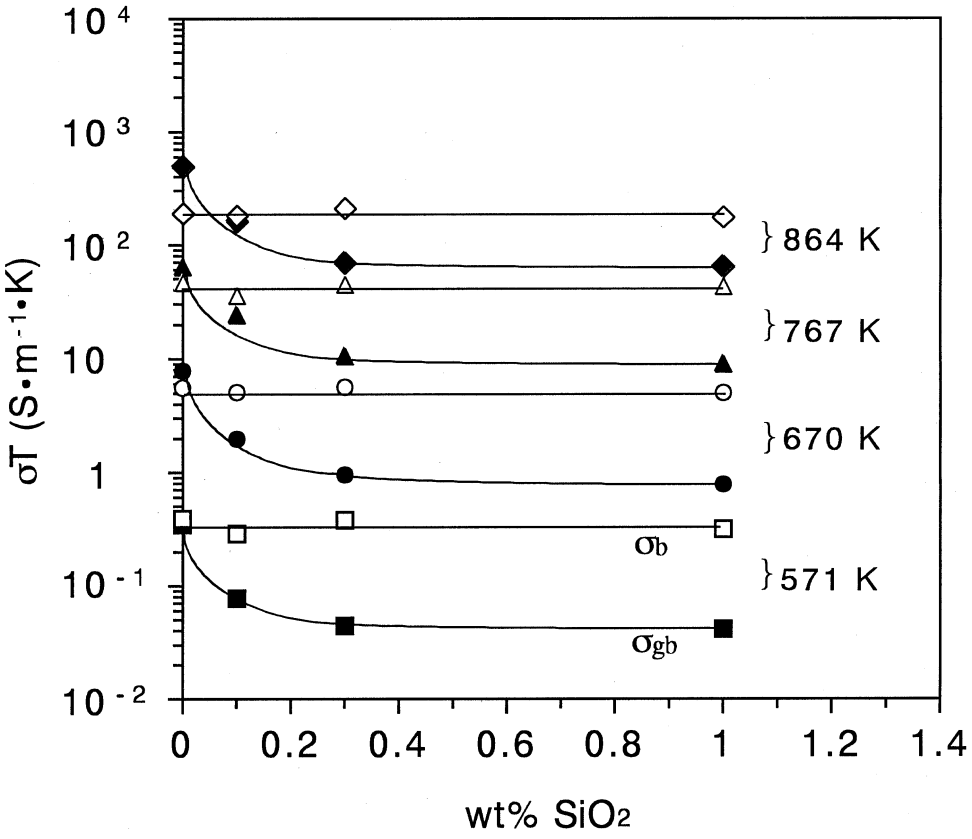

Fig. 5. Total bulk (open marks) and grain boundary (closed marks) conductivity changes versus silica content.

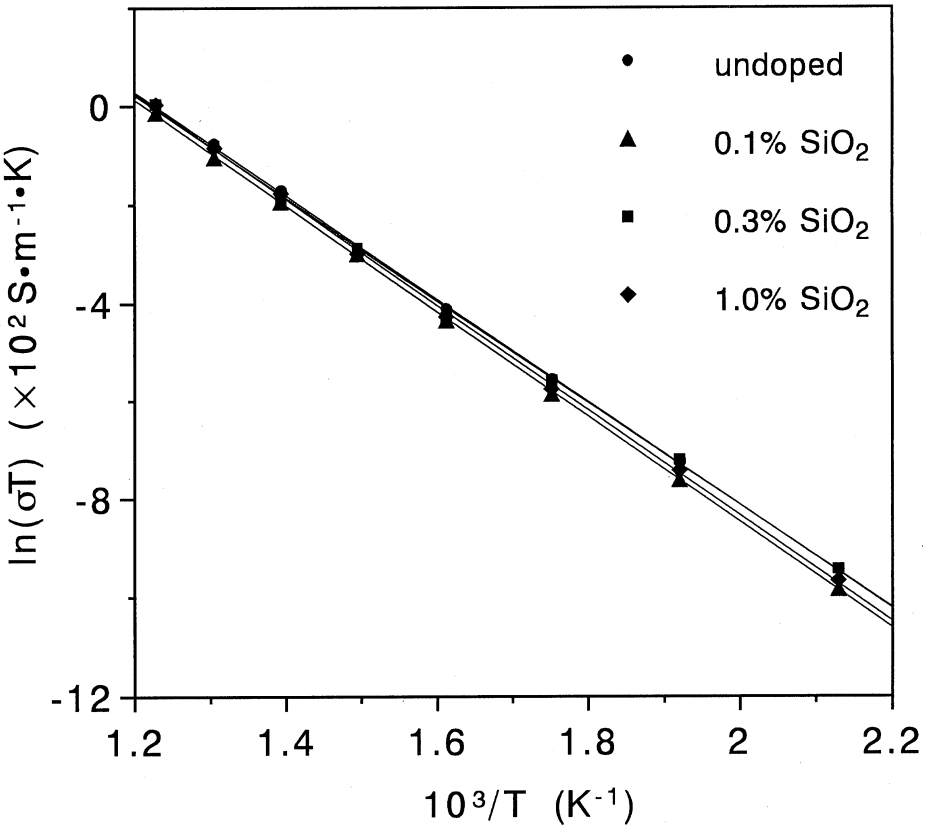

Fig. 6. Arrhenius plot of the total bulk conductivity.

the grain boundaries of the sample. The Z' and Z'' values in Fig. 4 are normalized by the division of lS, where l is the thickness of the sample and S the electrode area. Therefore the bulk and the grain boundary resistivity obtained from the intersection of the arcs with Z' axis in Fig. 4 are the total bulk and grain boundary resistivities (R_b and R_{gb}).

Figure 5 shows the total bulk and the grain boundary conductivity changes versus silica content. The total grain boundary conductivity $\sigma_{gb}(=1/R_{gb})$ of TZP decreased steeply for ≤ 0.3 wt % of silica doping and became nearly constant between 0.3–1.0 wt % of silica, while the total bulk conductivity $\sigma_b(=1/R_b)$ was constant between 0–1.0 wt % of silica. This result indicates that the grain boundary modification with silicon is completed by 0.3 wt % of silica doping. This result corresponds to the glass pocket formation, which was observed by SEM for the samples whose silica content is ≥ 0.5 wt %.

Figures 6 and 7 show the Arrhenius plots of the total bulk and grain boundary conductivities, respectively. The absolute values and slopes of the total bulk conductivity curves are similar for all the samples. Total grain boundary conductivity varies systematically with the amount of doped-silica, but the slopes of the Arrhenius plots of the grain boundary conductivity are similar for all the samples. The activation energies calculated from the Arrhenius plots are summarized in Table 1. These results are similar to the values reported by Gödickemeier (0.91–0.94 eV for the bulk conductivity and 1.10–1.18 eV for the grain boundary conductivity) for the silica-doped 3Y-TZP prepared by dry processing [18].

When the brick layer model is applied for the sintered samples, the specific bulk conductivity σ_b^{sp} and the specific grain boundary conductivity σ_{gb}^{sp} are given by [16]

$$\sigma_b^{sp} = \sigma_b \tag{5}$$

and

$$\sigma_{gb}^{sp} = \sigma_{gb} \cdot (\delta_{gb}/a) \tag{6}$$

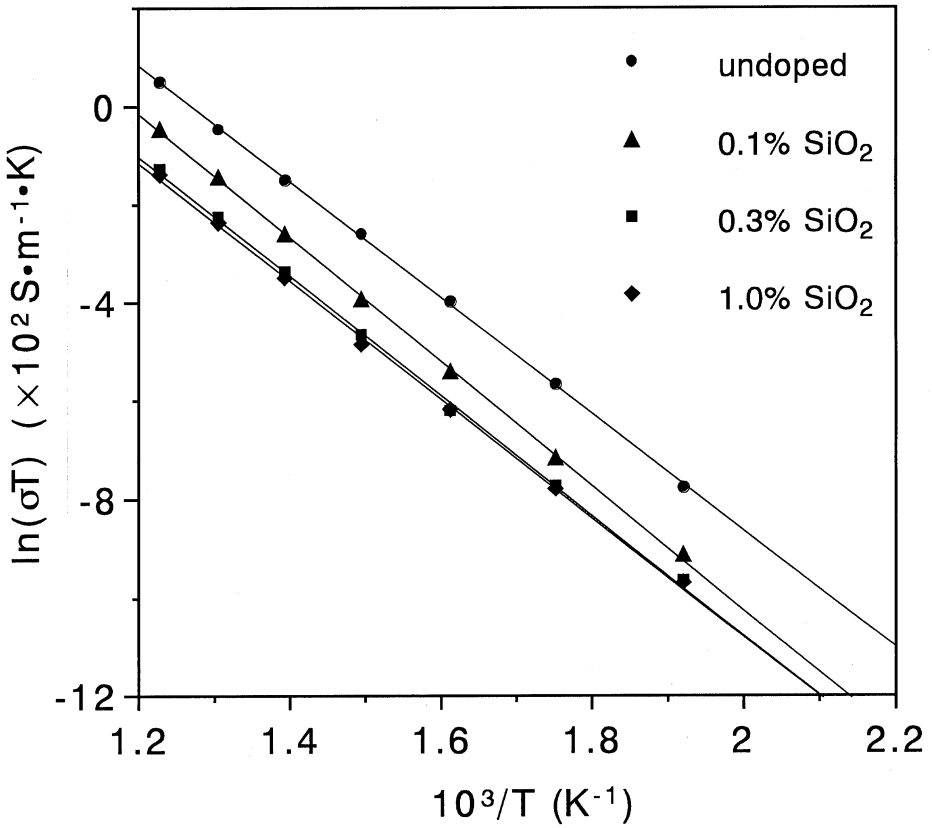

Fig. 7. Arrhenius plot of the total grain boundary conductivity.

where δ_{gb} is the effective electrical thickness of the grain boundary and a $(= 0.806d_g)$ is the edge length of the cubic grains. Using the total grain boundary capacitance $C_{gb}(= 1/(2\pi f R_{gb}))$ and the relative dielectric constant of the grain boundary ε_{gb}, δ_{gb} is given by

$$\delta_{gb} = \varepsilon_0 \varepsilon_{gb} \mathrm{a}/C_{gb} \tag{7}$$

where ε_0 is the permittivity of free space. Figure 8 shows $\delta_{gb}/\varepsilon_{gb}$ versus silica content. $\delta_{gb}/\varepsilon_{gb}$ is almost saturated to $\approx 5.7 \times 10^{-11}$m above ca. 0.3 wt % of SiO_2. This value is consistent with the value reported $(4.8 \sim 7.5 \times 10^{-11}\mathrm{m})$ for silica-doped 3Y-TZP [18]. If the thickness of the grain boundary δ_{gb} is given, the relative dielectric constant of the grain boundary can be estimated. Assuming that $\delta_{gb} = 0.8$ nm, then it can be estimated that $\varepsilon_{gb} = 14.0$ for the silicon-segregated grain boundary of 3Y-TZP. This value is higher than the relative dielectric constant of silica glasses (ca. $4 \sim 6$) [32], which suggests that the grain boundary phase must be different from a silica glass phase. At grain boundaries of 3Y-TZP, yttrium might be cosegregated with the silicon atoms [20,27].

The mechanical properties of the silica-doped 3Y-TZP prepared by colloidal processing are under investigation. The tensile elongation of the colloidally-processed samples is superior to that of the

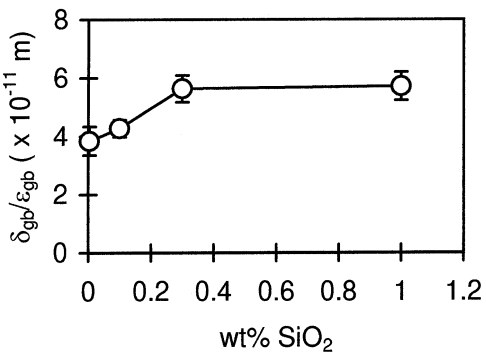

Fig. 8. The ratio of $\delta gb/\varepsilon gb$ versus silica content

conventionally produced material. The superiority of the superplasticity of colloidally-processed samples is attributed to the homogeneous distribution of SiO_2 and the fine grain size. The true fracture strain of TZP prepared by colloidal processing was found to be more than 40% higher than TZP prepared by dry processing [33].

4. Conclusions

The grain boundaries of 0–1.0 wt % silica-doped 3Y-TZP, prepared by colloidal processing, was studied by SEM observation and electrical conductivity measurements by complex impedance spectroscopy. The formation of glass pockets at multiple junctions was observed for $\geq$ 0.5 wt % silica-doped samples. The apparent grain boundary conductivity of TZP decreased steeply by the addition of $\leq$0.3 wt % of silica and became nearly constant between 0.3–1.0 wt % of silica. This result indicates that the grain boundary modification with silicon is saturated for silica contents over 0.3 wt %. The bulk conductivity was found to be constant between 0–1.0 wt % of silica doping.

Acknowledgment

The authors are grateful to K. Ozawa and T. S. Suzuki at NRIM for helpful advice on electrical conductivity measurements and SEM observation, and Y. Kaieda and N. Oguro at NRIM for help in sample preparation by CIP. This work was supported by special coordination fund from the Science and Technology Agency of Japan.

References

1. F. Wakai, S. Sakaguchi, and Y. Matsuno, *Advanced Ceramic Materials*, **1**, 259 (1986).
2. F. Wakai, S. Sakaguchi, and H. Kato, *J. Ceram. Soc. Jpn.*, **94**, 721 (1986).
3. F. Wakai, *Tetsu-to Hagané*, **75**, 389 (1989).
4. T. G. Nieh and J. Wadsworth, *Acta metall. mater.*, **38**, 1121 (1990).
5. M. J. Verkerk, A. J. A. Winnubst, and A.J. Burggraaf, *J. Mat. Sci.*, **17**, 3113 (1982).
6. M. Miyayama, H. Yanagida, and A. Asada, *Am. Ceram. Soc. Bull.*, **64**, 660 (1985).
7. K. Kajihara, Y. Yoshizawa, and T. Sakuma, *Acta metall. mater.*, **43**, 1235 (1995).
8. K. Hiraga, H. Y. Yasuda, and Y. Sakka, *Mater. Sci. Eng. A*, (in press).
9. C. H. Schilling and I. A. Aksay, *Engineered Materials Handbook Vol. 4*, *Ceramics and Grasses*, ASM International, pp. (1991), 153–160
10. F. F. Lange and K. T. Miller, *Am. Ceram. Soc. Bull.*, **66**, 1498 (1987).
11. F. F. Lange, *J. Am. Ceram. Soc.*, **72**, 3 (1989).
12. M. J. Verkerk, A. J. A. Winnubst, and A. J. Burggraaf, *J. Mat. Sci.*, **17**, 3113 (1982).
13. K. C. Radford and R. J. Bratton, *J. Mat. Sci.*, **14**, 66 (1979).
14. N. Bonanos, R. K. Sloywinski, B. C. H. Teele, and E. P. Butler, *J. Mat. Sci. Lett.*, **3**, 245 (1984).
15. S. Rajendran, J. Drennanm, and S. P. S. Badwal, *J. Mat. Sci. Lett.*, **6**, 1431 (1987).
16. S. P. S. Badwal and J. Drennan, *J. Mat. Sci.*, **22**, 3231 (1987).
17. F. T. Ciacchi, K. M. Crane, and S. P. S. Badwal, *Solid State Ionics*, **73**, 49 (1994).
18. M. Gödickemeier, B. Michel, A. Orliukas, P. Bohac, K. Sasaki, L. Gauckler, H. Heinrich, P. Schwander, G. Kostorz, H. Hofmann, and O. Frei, *J. Mater. Res.*, **9**, 1228 (1994).
19. G. Chiodelli, G. Flor, and M. Scagliotti, *Solid State Ionics*, **91**, 109 (1996).
20. M. Aoki, Y.-M. Chiang, I. Kosacki, J.-R. Lee, H. Tuller, and Y. Liu, *J. Am. Ceram. Soc.*, **79**, 1169 (1996).
21. M. C. Steil and F. Thevenot, *J. Electrochem. Soc.*, **144**, 390 (1997).
22. T. Uchikoshi, Y. Sakka, K. Ozawa, and K. Hiraga, *Mat. Res. Soc. Symp. Proc.*, **457**, 33 (1997).
23. T. Uchikoshi, Y. Sakka, and H. Okuyama, *J. Jpn. Soc. Powder and Powder Metall.*, **42**, 309 (1995).
24. T. Uchikoshi, Y. Sakka, and K. Ozawa, *Proc. 5th. World Congr. Chem. Eng.*, **IV**, 1007 (1996).
25. M. I. Mendelson, *J. Am. Ceram. Soc.*, **52**, 443 (1969).
26. K. C. Gradfoord and R. J. Bratton, *J. Mat. Sci.*, **14**, 59 (1979).
27. Y. Ikuhara, P. Thavorniti, and T. Sakuma, *Materials Science Forum*, **243–245**, 345 (1997).
28. M. Gust, G. Goo, J. Wolfenstine, and M. L. Mecartney, *J. Am. Ceram. Soc.*, **76**, 1681 (1993).
29. D. R. Clarke, *Ultramicroscopy*, **4**, 33 (1979).
30. C. D. Terwilliger and Y.-M. Chiang, *Acta metall. Mater.*, **43**, 319 (1995).
31. H. Schubert, *J. Am. Ceram. Soc.*, **69**, 270 (1986).
32. *CRC Handbook of Chemistry and Physics*, edited by D. R. Lide and H. P. R. Frederikse (CRC Press Inc., Boca Raton, 1997), p. 12–56.
33. Y. Sakka, T. Uchikoshi, K. Ozawa, K. Morita, H. Yasuda, and K. Hiraga, *Proc. US-Jpn. Workshop on Electrically Active Ceramic Interfaces*, (1998), p. 97.